JOURNAL OF CATALYSIS 111, 120–135 (1988)

Synthesis of Alcohols from Carbon Oxides and Hydrogen

VII. Preparation, Activation, and Catalytic Behavior of a ZnMnCrK-Oxide Catalyst

P. FORZATTI,[1] C. CRISTIANI, N. FERLAZZO, L. LIETTI, E. TRONCONI, P. L. VILLA, AND I. PASQUON

Dipartimento di Chimica Industriale ed Ingegneria Chimica "G. Natta" del Politecnico, Piazza Leonardo da Vinci, 32, I-20133 Milan, Italy

Received February 10, 1987; revised December 1, 1987

The preparation, activation, and catalytic behavior of a $Zn_1Mn_{1.1}Cr_{1.03}K_{2.06}$ oxide catalyst reported in the early literature for the synthesis of higher alcohols has been investigated by means of chemical analysis, XRD, IR, DTA-TG, SEM, surface area measurements, and flow reactor experiments. Evidence has been collected in support of the following points: (1) Reaction of basic carbonates of Zn and Mn with a solution of K_2CrO_4 at about 70–80°C (final pH 8.5) occurs through a redox mechanism; drying at ≈100°C of the resulting mass provides a catalyst precursor made of a core formed by a phase with a spinel structure and basic zinc carbonate covered by a shell of α-K_2CrO_4 and possibly $KHCO_3$. (2) Basic Zn carbonate and $KHCO_3$ are decomposed upon activation at 400°C. (3) The spinel-like phase is stable under N_2 upon activation at 400°C, whereas it is transformed into a phase with a rock salt-type structure, with related ZnO segregation, upon activation at 400°C in H_2; reoxidation in air induces the reverse transformation. (4) Calcination at 1000°C always gives rise to a phase with a tetragonal symmetry typical of $Zn^{II}Mn_2^{III}O_4$. A lumped kinetic treatment of the catalytic activity data indicates that this catalyst behaves similarly to a commercial ZnCrO catalyst impregnated with K_2O, but for an overall reduction of activity due to a lower surface area. Characterization of the catalyst after the activity runs provides data very similar to those obtained from the characterization of catalyst samples activated under a reducing atmosphere.

INTRODUCTION

Catalysts of industrial interest for the direct synthesis of methanol and higher alcohols from CO_x–H_2 mixtures generally belong to one of three classes: (i) alkali-promoted higher-temperature methanol synthesis catalysts (e.g., ZnO–Cr_2O_3 + K_2O); (ii) low-temperature copper-based methanol synthesis catalysts modified with alkali promoters (e.g., Cu–ZnO–Cr_2O_3 + K_2O, Cu–ZnO–Al_2O_3 + K_2O); (iii) modified Fischer–Tropsch catalysts (e.g., MoS_2–CoS + K_2O, alkalinized Cu–Co-based catalysts).

Interest in the direct synthesis of alcohols from CO_x and H_2 has grown recently since the mixture produced in this reaction has become attractive as a component for gasoline blends, particularly as an octane booster. The literature (*1–19*) provides an overview of the large volume of work that has been done on this subject in recent years. However, this reaction has been known for many years, and important contributions were published early (*20–27*). Among these, the work of Frohlich and coworkers (*20, 21*) deserves to be mentioned. These authors investigated several catalysts prepared by reacting different mixtures of basic carbonates of Zn and Mn with a solution of K_2CrO_4 and concluded that the optimal catalyst corresponds to the molar proportion $Zn_1Mn_{1.1}Cr_{1.03}K_{2.06}$ (*21*). This catalyst was used in a series of experiments aimed at investigating the controlling mechanism of formation of higher alcohols.

[1] Author to whom correspondence should be addressed.

0021-9517/88 $3.00

Nevertheless, the chemistry underlying the preparation and activation of the catalyst, as well as the nature of the gaseous products formed during the reaction, was not addressed properly. Indeed, a clear understanding of the preparation and activation steps could provide a basis for improved formulations of related catalyst systems. Also, the formation of gaseous products, namely CO_2, CH_4, and other hydrocarbons, is of great relevance to industrial implementation of a process for higher alcohol synthesis, where typically after condensation of the liquid products the gaseous stream is first washed of CO_2 and then recycled to the synthesis reactor (*4, 18, 19*).

In the present paper we report the results obtained during the investigation on the preparation and activation under different conditions of the catalyst precursor reported by Frohlich and Cryder. The catalytic behavior and the characterization of the catalyst discharged after activity runs are also addressed.

METHODS

Preparation and activation of the catalyst were investigated through the following steps: (i) preparation of the basic carbonates of Zn and Mn; (ii) reaction of basic carbonates of Zn and Mn with a solution of K-chromate, followed by drying at ≈100°C; (iii) activation at 400°C under inert (N_2) or reducing (H_2) atmospheres; (iv) calcination at 1000°C; (v) reoxidation of the reduced samples. Also, water was added to the sample dried at ≈100°C and an insoluble portion was separated from the solution. Both samples were dried at ≈100°C, and then activated at 400°C under N_2 or H_2 atmospheres; some were also calcined up to 1000°C. The sequence of operations involved in the preparation/activation study is summarized in Fig. 1 and described in the following. Samples in Fig. 1 and in the following text are identified with notations indicating the sample number, the activation temperature, and the corresponding atmospheres: e.g., II4H10A indicates sample II activated at 400°C under H_2 and further calcined at 1000°C.

Preparation of the basic carbonates. The basic carbonates of Zn and Mn were precipitated at room temperature (RT) from the solution of $Zn(NO_3)_2 \cdot 6H_2O$ (Carlo Erba RPE) and $Mn(NO_3)_2 \cdot 4H_2O$ (Fluka PPA) in the molar ratio 1 : 1.1, using a solution of $(NH_4)_2CO_3$ (20% w/w) and under stirring. The white precipitate (final pH 7.5) was washed, filtered, and dried at ≈100°C (sample I).

Reaction of the basic carbonates of Zn and Mn with the K-chromate solution. The basic carbonates of Zn and Mn were made into a thin paste with water, and a solution of K chromate was added at T = 70–80°C to obtain a catalyst with the final atomic ratio Zn/Mn/Cr/K = 1/1.1/1.03/2.06. The color of the suspended particles changed from white to yellowish and finally green-brownish. The precipitate was dark, and the pH of 8.5 was measured. The resulting mass was dried first on a hot plate, and then in an oven at ≈100°C; further repeated additions of water, followed by drying at ≈100°C, resulted in sample II1A. From a portion of this sample, after addition of water, filtration, and drying at ≈100°C, samples III1A and IV1A were obtained.

Activation at 400°C under inert or reducing atmosphere. Samples II1A, III1A, and IV1A were activated at 400°C (heating rate = 120°C/h, hold 2 h) under inert (N_2) or reducing atmospheres (H_2/N_2 mixture with hydrogen content increasing from 5% up to 100%), and then allowed to cool under N_2 down to RT by switching off the oven. The cooling typically lasted 12 h. When reducing atmospheres were used, before discharging at the open air the samples were exposed at RT to an atmosphere of slowly increasing oxygen content, from 0.1% up to 20%, to prevent pyrophoric effects.

Calcination at 1000°C. Samples III4N and II4N were activated in air at 1000°C (hold 2 h) and allowed to cool to RT by

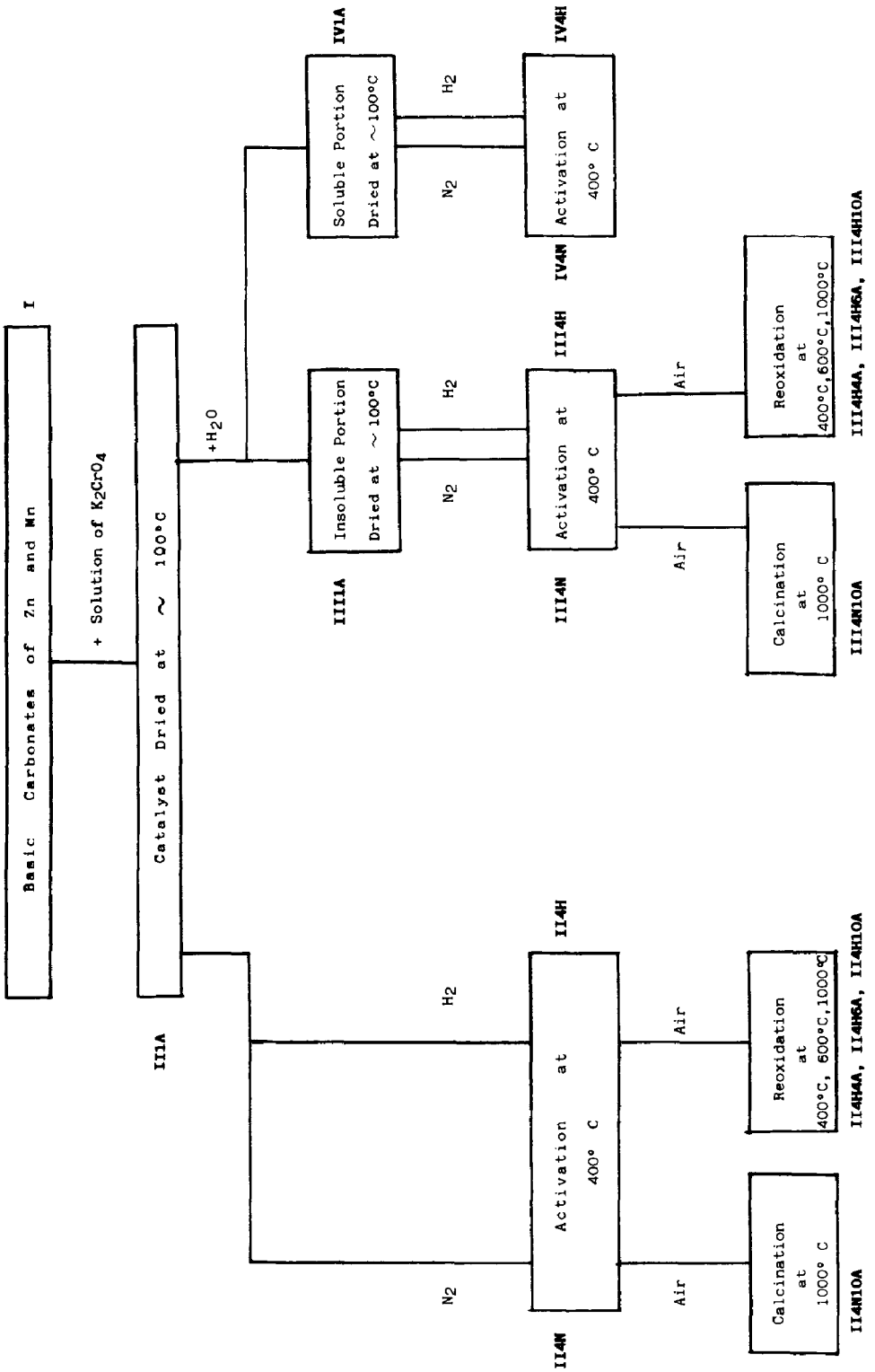

FIG. 1. Sequence of operations involved in the preparation and activation of the ZnMnCrK-oxide catalyst.

switching off the furnace. The cooling typically lasted 18 h.

Reoxidation of the reduced samples. Samples III4H and II4H were reoxidized in air at 400°C (hold 2 h), 600°C (hold 2 h), and 1000°C (hold 2 h). The cooling procedure specified above was followed.

Characterization of the catalyst samples. The samples were characterized by chemical analysis, X-ray diffraction, IR spectroscopy, DTA-TG, SEM, and surface area measurements.

Zn, Mn, and K contents were determined by atomic absorption using a Perkin–Elmer 303 instrument. The Cr content was measured by manganometric titration, and the CO_2 content was determined by gas evolution. X-ray powder diffraction patterns were collected using a Philips PW 1050/70 vertical goniometer and PW 1730 generator. IR spectra were recorded on a Perkin–Elmer 457 instrument with the KBr pressed disk technique. DTA-TG data were obtained with a Mettler 2000 instrument typically operating with a heating rate of 20°C/min.

A Jeol scanning electron microscope equipped with an X-ray microprobe was used to obtain information about the surface and bulk composition of the discharged catalyst. Catalyst surface areas were determined with a Carlo Erba Sorptomatic Series 1800 instrument with a BET dynamic system.

Flow reactor experiments. All catalytic activity runs were performed with the same catalyst sample (14.9 g) in a copper-lined tubular reactor at $P \approx 85$ atm using a H_2/CO = 2/1 feed mixture. A description of the experimental setup and the analytical procedures is given elsewhere (*8*). Due to difficulties in the quantitative gas chromatographic analysis of the reaction products, C_{2+} hydrocarbons were estimated from the H_2O balance by attributing to their formation the amount of $H_2O + CO_2$ exceeding that stoichiometrically corresponding to oxygenates and methane found among the products. Although approximate, this procedure enables an acceptable estimation of the catalyst selectivity to hydrocarbons, which has often been overlooked in previous studies concerned with higher alcohol synthesis. When the catalyst was discharged at the end of the activity runs, sticking of the particles was observed, due to the high content of K in the catalyst.

RESULTS AND DISCUSSION

Preparation of the Basic Carbonates of Zn and Mn

The first step in the preparation procedure consists of obtaining the basic carbonates of Zn and Mn.

Chemical analysis confirmed that Zn and Mn have been thoroughly precipitated, and that the CO_2 content (29%) was lower than would be expected (34%) if neutral carbonates had been obtained.

The XRD powder pattern is very close to that published in the literature for $MnCO_3$. The refined lattice parameters are a_0 = 4.733 Å, c_0 = 15.422 Å and the goodness of fit, expressed as R_w, is 9.6%. They compare very well with the values given for $MnCO_3$ (a_0 = 4.777 Å, c_0 = 15.67 Å) with a slight contraction in the direction of $ZnCO_3$ (a_0 = 4.651 Å, c_0 = 14.98 Å). The IR spectrum also gives evidence only of $MnCO_3$ rhodhocrosite (Sadtler Standard Spectrum 1754).

DTA-TG analysis under N_2 atmosphere showed two endothermic peaks (T_{max} = 270°C and 396°C), both with associated weight loss. These temperatures compare well with the decomposition temperatures of $Zn_5(OH)_6(CO_3)_2$ (T_{max} = 266°C) and $MnCO_3$ (T_{max} = 410°C). However, the weight loss associated with the first peak is smaller than that expected if the whole Zn had been present as basic zinc carbonate, whereas the opposite was measured for the second peak. This further suggests that Zn^{2+} ions have been partially incorporated in $MnCO_3$.

Altogether these data indicate that sample I1A is made up of a mixture of (Zn, Mn)CO_3 and $Zn_5(OH)_6(CO_3)_2$. The lack of

TABLE 1

Results of Chemical Analysis for Samples II1A, III1A, and IV1A

Sample[a]	Zn[b]		Mn[b]		Cr[c]		K[b]		CO_2[d]	
	Expected	Found	Expected	Found	Expected	Found	Expected	Found	Expected	Found
II1A	0.22	0.21	0.242	0.24	0.227	0.219	0.453	0.41	—	0.08
III1A	—	0.20	—	0.24	—	0.06	—	<0.01	—	0.016
IV1A	—	<0.01	—	<0.01	—	0.16	—	0.41	—	0.08

[a] Basis assumed for the mass balance calculation: 0.2 g atom of Zn.
[b] Atomic absorption.
[c] Manganometric titration.
[d] Gas evolution.

detection of the typical X-ray lines of $Zn_5(OH)_6(CO_3)_2$ may be due to the poor crystallinity of this phase, whereas the detection of the typical IR bands of this compound at 1380 and 1500 cm^{-1} is prevented by the strong absorption of $MnCO_3$ in the same region.

It is worth noting that when zinc carbonate is precipitated in the absence of Mn at the same pH value (7.5), $Zn_5(OH)_6(CO_3)_2$ is observed in both XRD and IR spectra, with only traces of $Zn_4(OH)_6CO_3 \cdot H_2O$, in line with literature data (*28*).

Reaction of the Basic Carbonates of Zn and Mn with the K-Chromate Solution

Table 1 shows the results of the chemical analysis of samples II, III, and IV dried at ≈100°C.

The insoluble portion (sample III1A) contains all of the Zn and Mn, approximately one-third of Cr, traces of K, and small amounts of CO_2 as compared with the stoichiometric quantities measured in sample II.

The X-ray pattern of III1A (Fig. 2) shows

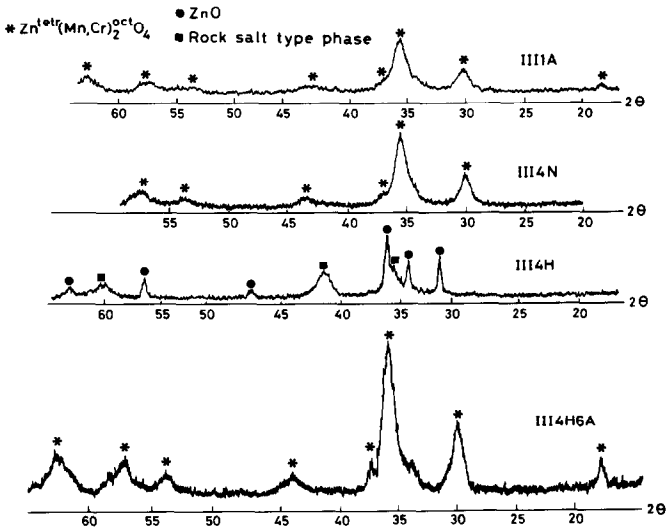

FIG. 2. X-Ray diffraction patterns of the insoluble portion dried at ≈100°C and after activation under different conditions.

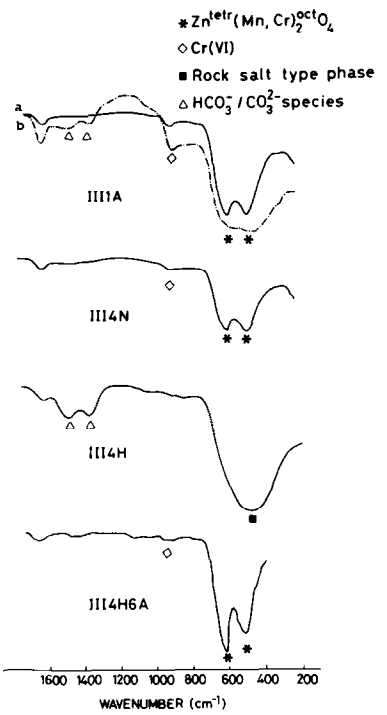

FIG. 3. IR spectra of the insoluble portion dried at ≈100°C and after activation under different conditions (sample III1A): (a) typical (full line) and (b) enhanced (dashed line) loading.

only the characteristic peaks of a phase with a spinel structure, isotypic with $ZnCr_2O_4$ (ASTM Fiche 22-1007). The calculated cell parameter (a = 8.34 Å) is slightly higher than the value reported in the literature for $ZnCr_2O_4$ (a = 8.3275 Å), which indicates a small expansion of the unit cell.

The IR spectrum of III1A (Fig. 3) shows (i) a couple of bands at 500 and 600 cm^{-1}, attributable to the presence of a phase with a spinel structure (*29*); (ii) a weak band at about 930 cm^{-1} associated with Cr(VI) in small amounts (*30*); (iii) a couple of bands at 1350 and 1500 cm^{-1}, barely manifest, which can be associated with the presence of the basic carbonate of Zn in small amounts (Sadtler Standard Spectrum 1743). The characteristic bands of $MnCO_3$/(Zn, Mn)CO_3 at 1400 cm^{-1} were absent.

The DTA-TG curves in N_2 and H_2 of III1A are given in Fig. 4. A small weight loss was recorded under inert atmosphere above 200°C (Fig. 4a), and can be attributed to the decomposition of $Zn_5(OH)_6(CO_3)_2$. An additional complex process globally exothermic with associated weight loss at T > 200°C was measured only under H_2 (Fig. 4b), and can be related to the reduction of Mn^{3+} to Mn^{2+} accompanied by a phase transition from a spinel-like to a rock salt-type structure (see below). In line with IR results, no decomposition process of $MnCO_3$/(Zn,Mn)CO_3 is evident.

The above results suggest that the reaction between the basic carbonates of Zn and Mn and the K-chromate solution proceeds according to the redox mechanism

$$3Mn^{2+} + Cr^{6+} \rightarrow 3Mn^{3+} + Cr^{3+}$$

to the almost complete consumption of Mn^{2+}. This picture is consistent with (a) the complete consumption of $MnCO_3$/(Zn,Mn)CO_3 evidenced by DTA-TG and IR measurements; (b) the content of Cr in sample III1A; (c) the presence of a phase with a spinel structure slightly expanded as compared with $ZnCr_2O_4$ [the ionic radii ($Zn^{2+(IV)}$

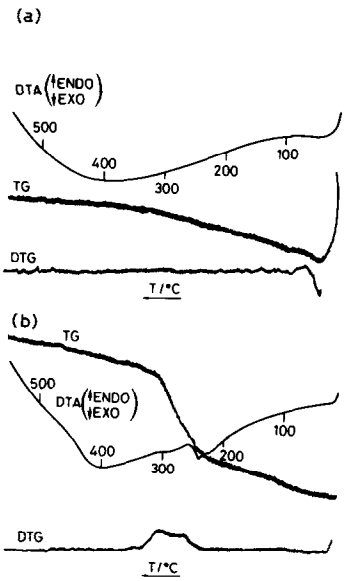

FIG. 4. DTA-TG curves of the insoluble portion dried at ≈100°C (sample III1A): (a) in N_2, (b) in H_2.

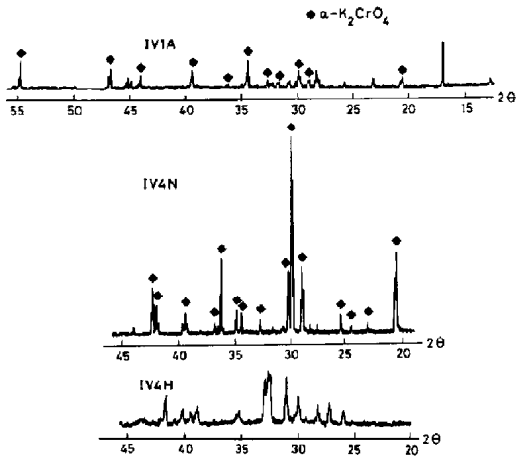

FIG. 5. X-Ray diffraction patterns of the soluble portion dried at ≈100°C and after activation at 400°C in N_2, H_2.

= 0.74; $Zn^{2+(VI)}$ = 0.89; $Mn^{3+(VI)}$ = 0.785; $Cr^{3+(VI)}$ = 0.755 Å) and the octahedral site preference energies (Zn^{2+} = −31.6; Mn^{3+} = 3.1; Cr^{3+} = 16.6 kcal/g atomic weight) (*31*, *32*) indeed suggest the structural formula $Zn^{TETR}[Mn^{III},Cr^{III}]_2^{OCT}O_4]$; (d) the presence of residual amounts of $Zn_5(OH)_6(CO_3)_2$ not involved in the formation of the phase with the spinel structure.

The chemical analysis of sample IV1A confirmed that the soluble fraction contains two-thirds of the chromium [in the form of Cr(VI)], almost the whole amount of K, and part of the CO_2 as compared with the corresponding quantities in sample II, whereas Zn and Mn are almost absent. The XRD pattern of IV1A (Fig. 5) shows the characteristic lines of α-K_2CrO_4 together with other unidentified peaks. The IR spectrum (Fig. 6) confirms the presence of α-K_2CrO_4 as well as of carbonate/bicarbonate species. The DTA-TG curves of sample IV1A are given in Fig. 7. The continuous weight loss between 100 and 200°C is possibly associated with the decomposition of $KHCO_3$. The complex effect, globally exothermic, with associated weight loss measured only under reducing atmosphere and above 450°C can be related to the reduction of α-K_2CrO_4.

On the whole the data referring to sample

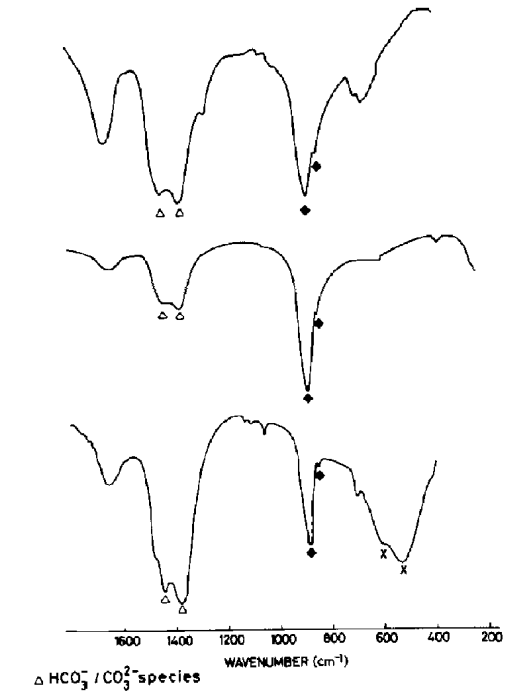

FIG. 6. IR spectra of the soluble portion dried at ≈100°C, and after activation at 400°C in N_2, H_2: IV1A (top), IV4N (middle), IV4H (bottom).

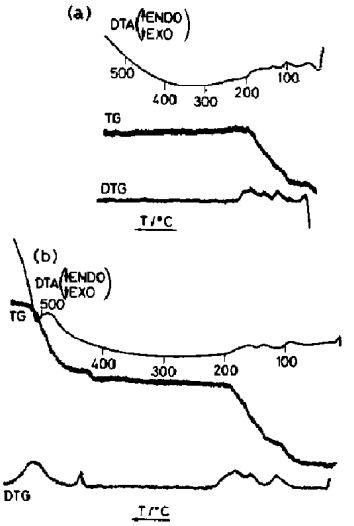

FIG. 7. DTA-TG curves of the soluble portion dried at ≈100°C (sample IV1A): (a) in N_2, (b) in H_2.

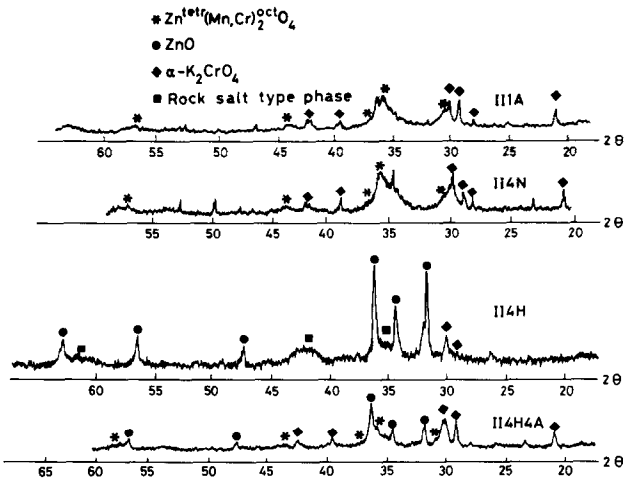

FIG. 8. X-Ray diffraction patterns of the untreated catalyst precursor dried at ≈100°C and after activation under different conditions.

IV1A confirm that Cr that has not reacted according to the redox reaction proposed above is present in the solution in the form of Cr(VI), and that drying of the solution at ≈100°C results in the appearance of α-K_2CrO_4 and in the formation of possibly $KHCO_3$.

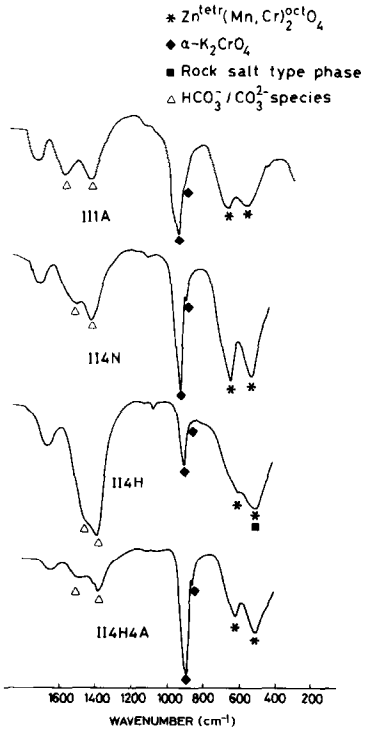

FIG. 9. IR spectra of the catalyst precursor dried at ≈100°C and after activation under different conditions.

The chemical analysis of sample III1A (Table 1) and the XRD and IR characterizations (Figs. 8, 9) confirm that it is a mixture of samples III1A and IV1A. The DTA-TG curves of sample III1A (Fig. 10) exhibit a continuous weight loss extending to 400°C, without marked thermal effects, which can be related to the decomposition of both $KHCO_3$ and $Zn_5(OH)_6(CO_3)_2$. Two exothermic peaks at 410 and 470°C were measured only under reducing atmosphere. Such peaks are associated with the reduction of Mn^{3+} and Cr^{6+} and occur at temperatures different from those observed for samples III1A and IV1A, possibly because of different sample morphology and/or interaction between the components.

Based on the solubility of the different species, and the drying procedure of the slurry, it seems reasonable to hypothesize that sample III1A is made of a core formed by $Zn^{TETR}(Mn^{III},Cr^{III})_2^{OCT}O_4$ + $Zn_5(OH)_6(CO_3)_2$ covered by a shell made of α-K_2CrO_4 and $KHCO_3$. Indeed, X-ray microprobe inspection of the sample after activity runs confirmed that the surface is enriched with Cr and K (see below).

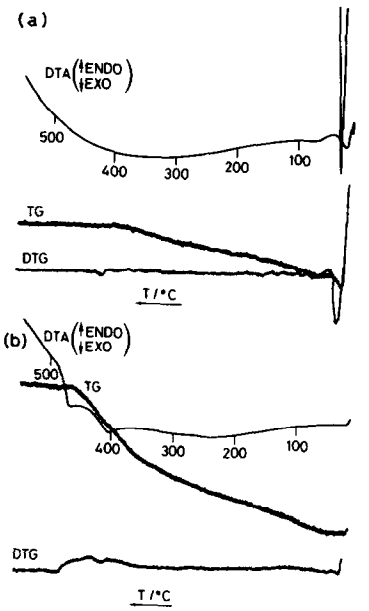

FIG. 10. DTA-TG curves of the untreated catalyst precursor dried at ≈100°C (sample II1A): (a) in N_2, (b) in H_2.

Activation of the Catalyst Precursor at 400°C under N_2

The X-ray pattern (Fig. 2) and the IR spectrum (Fig. 3) of sample III4N show the presence of a spinel-like phase $Zn(Mn,Cr)_2O_4$ practically unaltered compared with that observed at ≈100°C (a = 8.34 Å; a couple of IR bands at 500 and 600 cm^{-1}), the presence of Cr(VI) (IR band at ≈930 cm^{-1}), and the decomposition of the residual amount of $Zn_5(OH)_6(CO_3)_2$ (absence of IR absorption bands in the region 1300–1500 cm^{-1}). Also, no crystalline ZnO was detected by X-ray diffraction.

X-Ray and IR data for sample IV4N (Figs. 5, 6) show the presence of well-crystallized α-K_2CrO_4. A marked decrease in carbonate/bicarbonate species is also apparent based on comparison of the relative intensities of the characteristic IR bands. This can be associated with the decomposition of $KHCO_3$, which is expected to occur between 100 and 200°C, from the DTA-TG results already discussed in the previous section.

The characterization of sample II4N (Figs. 8, 9) confirms that it is actually a mixture of samples III4N and IV4N.

The bulk of these data indicates that activation at 400°C under N_2 results in decomposition of both $KHCO_3$ and $Zn_5(OH)_6(CO_3)_2$, whereas the phase with a spinel structure and α-K_2CrO_4 are almost unaltered.

Activation of the Catalyst Precursor at 400°C under H_2

XRD and IR data of the insoluble portion activated under H_2 at 400°C (sample III4H in Figs. 2 and 3) show the transformation of the spinel-like phase into a rock salt-type phase (a = 4.35 Å; characteristic IR band centered at about 500 cm^{-1}), together with the appearance of crystalline ZnO. Crystalline ZnO, which is formed under reducing atmosphere and not under inert atmosphere, is likely to originate from segregation of Zn^{2+} ions from the spinel-like phase $Zn^{TET}[Cr,Mn]_2^{OCT}O_4$, due to phase transition. Small amounts of carbonate–bicarbonate species are also evident, whereas Cr(VI) is absent.

Characterization of sample IV4H (Figs. 5, 6) showed (i) the disappearance of the characteristic XRD lines of α-K_2CrO_4; (ii) the appearance of new unidentified XRD peaks, and a new IR band at 540 cm^{-1} with a shoulder at 600 cm^{-1}, which can be assigned to reduced Cr(VI) species; (iii) the presence of an IR band at 890 cm^{-1} with a lower relative intensity, associated with CrO_4^{2-} species. Carbonate/bicarbonate species were also detected (IR bands at 1500–1300 cm^{-1}).

These data indicate that activation of the soluble portion at 400°C under H_2 results in reduction of α-K_2CrO_4, which is also in line with DTA-TG data discussed in the previous section.

XRD and IR spectra of sample II4H (Figs. 8, 9) confirm that it is actually a mixture of III4H and IV4H; only the reduced

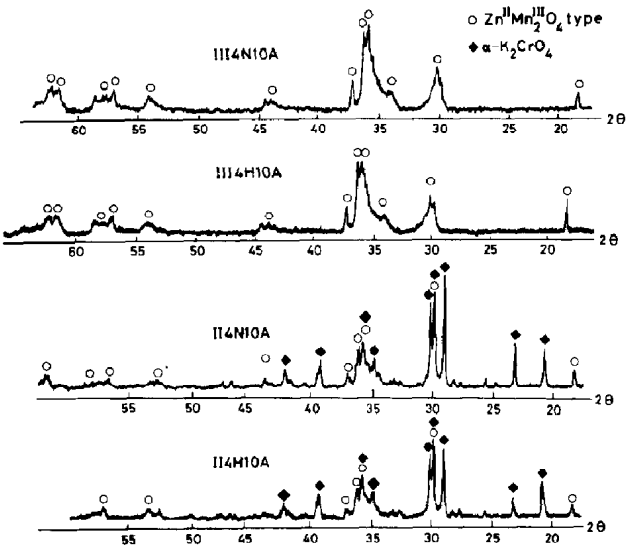

FIG. 11. X-Ray diffraction patterns of the catalyst precursor and of the insoluble portion after calcination at 1000°C.

phase of α-K_2CrO_4 appears to be less crystalline, as suggested by the absence of the characteristic XRD lines.

Calcination of the Catalyst Precursor at 1000°C

This treatment was given to samples III4N and II4N to study the thermal stability under oxidizing conditions of the catalyst precursor.

The XRD and IR spectra of III4N10A and II4N10A are presented in Figs. 11 and 12, respectively. It is apparent that calcination at high temperatures produces a distortion of the original phase, with a spinel structure from a cubic symmetry toward a tetragonal symmetry due to the Jahn–Teller distortion induced by the octahedral coordination of Mn^{3+} ions. This results in an X-ray pattern resembling that of $Zn^{II}Mn_2^{III}O_4$, which presents a tetragonal structure (ASTM Fiche 24-1133), and in a couple of characteristic IR bands at 515 and 620 cm^{-1}.

Reoxidation of the Samples Activated under H_2

Reoxidation with air at 600°C of sample III4H induces the reverse transformation

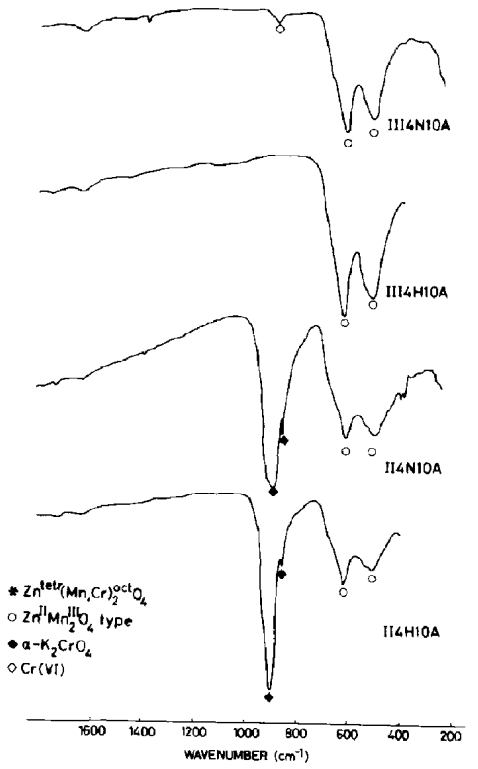

FIG. 12. IR spectra of the catalyst precursor and the insoluble portion after calcination at 1000°C.

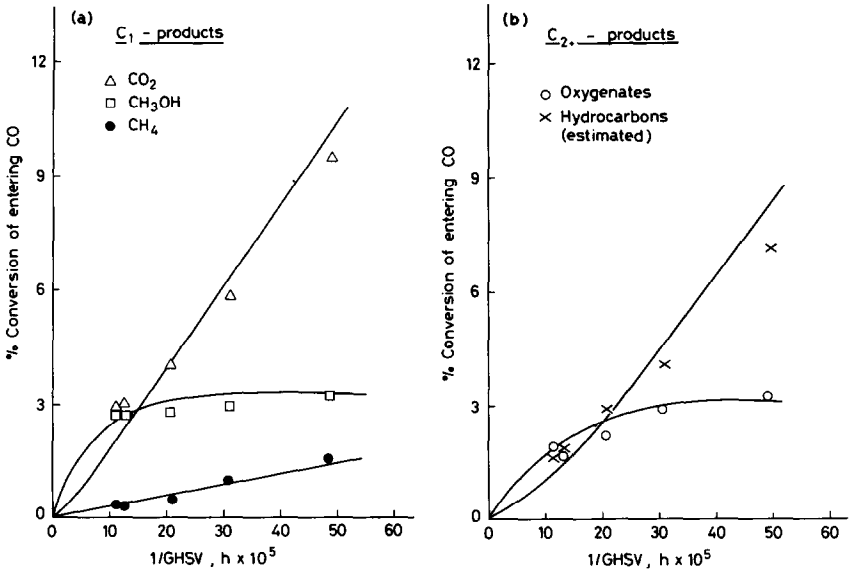

FIG. 13. Effect of contact time on C_1 products (a) and C_{2+} products (b) obtained from CO and H_2. Reaction conditions: T = 400°C, P = 85 atm, H_2/CO = 2/1.

from the rock salt-type phase to the spinel-like phase (a = 8.36 Å), with the lattice reincorporation of crystalline ZnO. This is clearly shown by XRD and IR data (Figs. 2, 3); Cr (VI) species are also formed in small amounts. The partial reincorporation of Zn^{2+} ions is observed already at 400°C, where larger amounts of Cr(VI) species are detected by IR.

Transformation from the rock salt-type structure to the spinel phase and the associated reincorporation of ZnO were also observed by reoxidizing sample II4H at 400°C (Figs. 8, 9).

Further oxidation of both samples III4H and II4H at 1000°C induces a distortion of the spinel structure from the cubic symmetry toward a tetragonal symmetry (Figs. 11, 12), in analogy with the results already discussed for samples III4N10A and II4N10A.

Flow Reactor Experiments

During the activity runs a large variety of products were identified, including methanol, water, CH_4, CO_2, a few higher saturated and unsaturated hydrocarbons such as ethane and ethylene, and C_2–C_8 linear and branched alcohols. Among these, 1-propanol and isobutanol were present in the greatest amounts. Aldehydes, and to a lesser extent ketones and esters, were also detected.

The results of the runs exploring the effect of the space velocity are presented in lumped form in Fig. 13. It is apparent that the formation of methanol is faster than the formation of alcohols. With growing residence time methanol tends to the concentration corresponding to chemical equilibrium, while the percentage of CO converted to alcohols eventually equals that converted to methanol. Such behavior is in line with a stepwise reaction pattern where methanol formation is fast, and C_{2+} alcohols are formed by a slow condensation of CH_3OH-related C_1 adsorbed species followed by faster C_1 β-additions.

The selectivity of CO to CH_4 and higher hydrocarbons is relevant. The origin of higher hydrocarbons is not completely understood yet: their formation could possibly be explained by invoking a Fischer–

Tropsch reaction, or a consecutive dehydration of alcohols, or a combination of both mechanisms.

Finally, it should be noted that the consumption of CO to CO_2 soon becomes predominant as the contact time is increased. Thermodynamic considerations confirm that the CO_2 content in the reaction products also approaches the chemical equilibrium value of the water–gas shift reaction.

The curves for methanol and C_{2+} oxygenates in Fig. 13 are similar in shape to those reported by Frohlich and Cryder. However, these authors observed greater CO conversions to methanol (≈4.5%) and to higher alcohols (≈10.5%) because of the higher reaction pressure (200 atm versus 85 atm in this work).

Concerning the distribution of alcohols observed among the reaction products, the percent conversion of CO follows the order C_{5+} alcohols > propanols > butanols > ethanol, like most of the data reported by Frohlich and Cryder.

In Fig. 14 the effect of temperature on the main classes of reaction products is illustrated. An increased temperature promotes the formation of all species but methanol, whose concentration exhibits a maximum. The subsequent drop at higher temperatures likely results from both the temperature dependence of the controlling thermodynamics and the enhanced formation of heavier products.

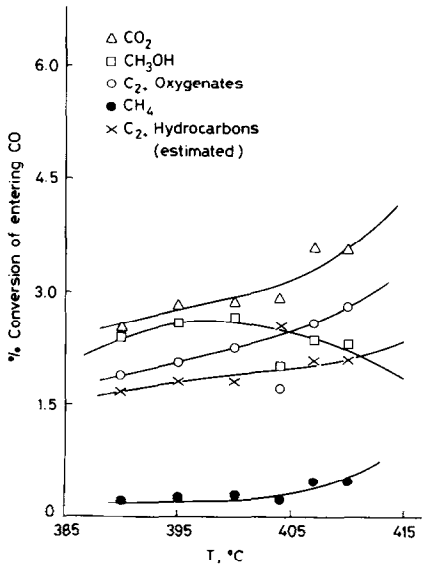

FIG. 14. Effect of temperature on the products obtained from CO and H_2. Reaction conditions: P = 85 atm, GHSV = 8000 h^{-1}, H_2/CO = 2/1.

A single run was performed at T = 400°C and GHSV = 8000 h^{-1} with 3% CO_2 added to the feed mixture. A significant drop in the yield of C_{2+} products was observed, the corresponding higher alcohol productivity falling from about 40 to about 8 g/h L_{cat}. A similar effect had been noted over a ZnCrKO catalyst (*8*), and can be explained by the inhibiting action of water directly experienced by Frohlich and Cryder if one considers that the addition of CO_2 to the feed results in the formation of H_2O due to the reverse water–gas shift reaction.

Kinetic Analysis

The data demonstrating the effect of space velocity (Fig. 13) have been given the same lumped treatment previously applied to a more extended set of activity data obtained over a commercial ZnCrO catalyst impregnated with 3% K_2O (*8*). According to the following approximate kinetic analysis, whose detailed development is discussed in Ref. (*8*), the complex reaction network of the higher alcohol synthesis is described on the basis of the five following reactions (or pseudoreactions):

$$CO + 2H_2 \leftrightarrow CH_3OH \quad (1)$$

$$CH_3OH + (N_c - 1)CO + 2(N_c - 1)H_2 \rightarrow HA + (N_c - 1)H_2O \quad (2)$$

$$CO + H_2O \leftrightarrow CO_2 + H_2 \quad (3)$$

$$CO + 3H_2 \rightarrow CH_4 + H_2O \quad (4)$$

$$HA \rightarrow OL + H_2O \quad (5)$$

Here, HA and OL are two pseudocomponents representative of an alcohol with N_c carbon atoms and of an olefin with N_c carbon atoms, respectively. The rate expres-

sions associated with each reaction step are as follows:

$$r_1 = k_1(p_{CO}p_{H_2}^2 - p_{CH_3OH}/K_1) \quad (6)$$

$$r_2 = k_2 p_{CH_3OH}/(1 + K_W p_{H_2O}) \quad (7)$$

$$r_3 = k_3(p_{CO}p_{H_2O} - p_{CO_2}p_{H_2}/K_3) \quad (8)$$

$$r_4 = k_4 p_{H_2} \quad (9)$$

$$r_5 = k_5(p_{HA})^{1/2} \quad (10)$$

The rate equations contain six adaptive parameters. The two appearing in r_2 (k_1, K_W) are heavily correlated, since both contribute to determine the rate of alcohol formation. In the present work the parameter K_W was fixed at the same value estimated for the ZnCrKO catalyst (8.84 atm^{-1}. Based on the analysis of the products of all runs the average carbon number N_c of the C_{2+} oxygenated products was found not very sensitive to the operating conditions, and the mean value (4.0) was used in the calculations. A pseudohomogeneous, isothermal plug-flow reactor model was assumed, and the parameter estimates obtained by multiresponse nonlinear regression (*8*). An adequate fit of the experimental data was achieved after the optimization procedure, resulting in average percentage errors in the range 7–15% for all responses. These were the outlet mole fractions of the observable products, namely, CH_3OH, C_{2+} oxygenates, CO_2, CH_4, and H_2O. Based on independent estimates of the experimental error and on the degree of approximation involved in the analysis, this level is regarded as acceptable. The goodness of fit can be visually evaluated from Fig. 13, where the solid lines represent model predictions of percentage CO converted to various products.

The calculated estimates of the kinetic parameters are reported in Table 2, where they are compared with the corresponding estimates obtained over the ZnCrKO catalyst (*8*). The surface areas of the two catalysts after activity runs are also given. It is apparent by inspection of Table 2 that the ratios of the kinetic parameters of the two catalyst are close to the ratio of the surface areas, the only exception being the rate constant of methanol formation. This estimate, however, is ill-determined, since chemical equilibrium is already approached even at the highest space velocity.

Thus, the results of the kinetic analysis indicate that the activity data for the ZnMnCrK-oxide system can be rationalized within the same kinetic treatment previously applied to data obtained over a ZnCrKO catalyst, which suggests a more general validity of that approach. The observed differences in the estimates of the kinetic constants provide evidence that the catalyst specific surface area plays an important role in the higher alcohol synthesis, higher areas favoring greater yields of alcohols.

Characterization of the Catalyst after Activity Runs

X-ray diffraction patterns of the catalyst after activity runs are presented in Fig. 15 (sample A). As a reference, the XRD spec-

TABLE 2

Parameter Estimates for the Lumped Kinetic Model of Higher Alcohol Synthesis, Eqs. (6)–(10)

Catalyst	k_1	k_2	k_3	k_4	k_5	K_W	BET surface area[a] (m^2/g)
ZnCrMnKO (present work)	3.5×10^{-8}	2.0×10^{-3}	5.1×10^{-4}	3.4×10^{-6}	8.1×10^{-4}	8.84	15.3
ZnCrO + (*8*)	4.3×10^{-7}	3.0×10^{-3}	1.3×10^{-3}	1.0×10^{-5}	9.7×10^{-4}	8.84	41.

[a] Measured after activity runs.

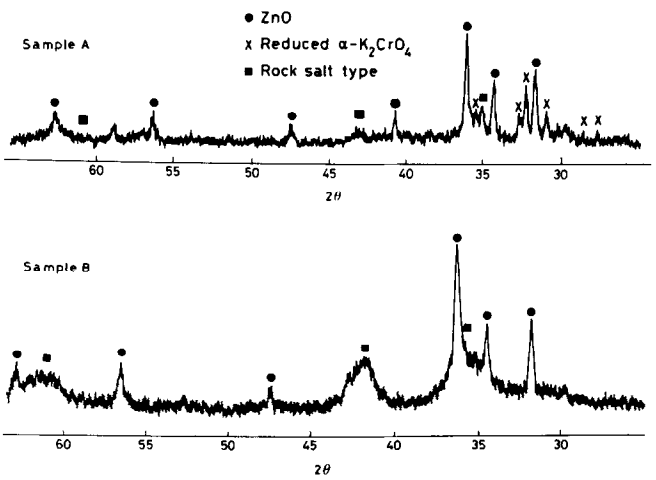

FIG. 15. X-ray diffraction patterns performed after activity runs of the ZnCrMnKO catalyst (sample A) and of the catalyst obtained by removing the soluble portion of the precursor (sample B).

trum recorded after an activity run of the sample obtained by washing the catalyst precursor in order to remove the soluble portion (α-K_2CrO_4 and carbonate species) is also presented in the same Figure (sample B). For both samples, crystalline ZnO and a phase with a rock salt-type structure (estimated cell parameter a = 4.4 Å for sample A, a = 4.3 Å for sample B) are evident. Sample A exhibits additional lines, which can be associated with the presence of α-K_2CrO_4 and with reduced α-K_2CrO_4 materials (see Fig. 4).

The IR spectra showed a broad absorption centered at 500 cm^{-1}, associated with a rock salt-type phase and with reduced Cr^{6+} species, and a shoulder at 600 cm^{-1}, which reveals a partial reoxidation of the sample due to an incipient rock salt-type → spinel-like phase transformation. All of these data are in line with results of the characterization work performed on similar samples activated under H_2 at 400°C.

Table 3 shows the results of the chemical analysis performed by X-ray microprobe inspection on the discharged catalyst pellets and on the same pellets finely ground. The results indicate that the surface layers (depth ≤ 1 μm) are enriched with both K and Cr. This is in agreement with the expectations based on the catalyst preparation and activation procedures discussed in previous paragraphs.

On the whole, these data indicate that under reaction conditions the catalyst consists of a core made mainly of a rock salt-type phase and crystalline ZnO, and of a surface enriched with Cr and K.

CONCLUSIONS

The present work enabled us to reach the following conclusions:

1. The procedure adopted for the preparation of basic carbonates of Zn and Mn results in a mixture of $(Zn,Mn)CO_3$ and $Zn_5(OH)_6(CO_3)_2$.

2. The reaction between the basic carbonates of Zn and Mn and the K_2CrO_4 solution involves the redox mechanism

TABLE 3

Results of the Analysis by X-Ray Microprobe on the Discharged Catalyst

	Cr/K	Mn/K	Zn/K
Catalyst pellets after activity runs (14–20 mesh)	0.49	0.38	0.17
Ground pellets (>325 mesh)	0.57	0.64	0.285

$$3Mn^{2+} + Cr^{6+} \rightarrow 3Mn^{3+} + Cr^{3+}$$

and proceeds to the almost complete consumption of Mn^{2+}. A spinel-like phase with the formula $Zn^{2+TETR}(Mn^{3+},Cr^{3+})_2^{OCT}O_4$ is formed already at this stage.

3. The catalyst precursor obtained after drying at ≈100°C is made of a core formed by the spinel-like phase and basic zinc carbonate covered by a shell of α-K_2CrO_4 and possibly $KHCO_3$.

4. Activation at 400°C in N_2 results in the decomposition of both $KHCO_3$ and $Zn_5(OH)_6(CO_3)_2$, the phase with the spinel structure and α-K_2CrO_4 being practically unaltered. Further calcination at 1000°C induces a distortion in the spinel phase from a cubic symmetry toward a tetragonal symmetry, typical of $Zn^{II}Mn_2^{III}O_4$.

5. Activation at 400°C in H_2 results in the reduction of Mn^{3+} to Mn^{2+} with a phase transformation from a spinel-like to a rock salt-type structure and related ZnO segregation, as well as in the reduction of α-K_2CrO_4. The phase with the rock salt structure is pyrophoric.

6. Reoxidation of the reduced samples at 600°C results in reincorporation of ZnO and in the related reverse phase transformation from the rock salt-type structure to the spinel structure. Further calcination at 1000°C induces a distortion of the spinel-like phase toward a tetragonal symmetry.

7. In flow reactor experiments the ZnMnCrK-oxide catalyst was found to promote the direct synthesis of methanol and higher alcohols from CO and H_2, in line with early data. Remarkable selectivities to gaseous products (CO_2, CH_4, C_{2+} hydrocarbons) were also observed.

8. The activity data could be described on the basis of a lumped kinetic scheme including five individual reaction steps, namely, formation of methanol and water–gas shift reaction (both limited by chemical equilibrium), chain growth to higher alcohols, methanation, and formation of higher hydrocarbons. Comparison with the results of a similar kinetic treatment of activity data obtained over a ZnCr-oxide catalyst promoted with 3% K_2O indicates a similar behavior of the two catalytic systems, the greater activity of the latter resulting apparently from a higher specific surface area.

9. Characterization of the ZnMnCr-oxide catalyst after activity tests has shown the presence of crystalline ZnO and of a phase with a rock salt-type structure. In addition, the surface is enriched with Cr and K.

ACKNOWLEDGMENT

This work was performed under a contract from Progetto Finalizzato Energetica II.

REFERENCES

1. Ichikawa, M., *Bull. Chem. Soc. Japan* **51,** 2273 (1978); Ichikawa, M., and Shikakura, K., *Stud. Surf. Sci. Catal.* **7,** 925 (1981); Ichikawa, M., *Chemtech,* 674 (1981); Ichikawa, M., Fukushima, T., and Shikakura, K., *in* "Proceedings, 8th International Congress on Catalysis, Berlin," Vol. II, p. 69, Dechema, Frankfurt, 1984; Ichikawa, M., and Fukushima, T., *J. Chem. Soc. Chem. Commun.,* 321 (1985).
2. Klier, K., *in* "Catalysis of Organic Reactions" (W. R. Moser, Ed.), Dekker, New York, 1980; Vedage, G. A., Himelfarb, P., Simmons, W. G., and Klier, K., *Prepr. Petrol. Div. Amer. Chem. Soc.* **28,** 1261 (1983); "Catalytic Conversion of Synthesis Gas and Alcohols to Chemicals" (R. G. Herman, Ed.), Plenum, New York, 1984.
3. Pillai, G. C., Wei, T. C. J., and Stiles, A., Center for Catalytic Science and Technology, University of Delaware, Interim Report, 1981.
4. Courty, P., Duran, D., Freund, E., and Sugier, A., *J. Mol. Catal.* **17,** 241 (1982); Courty, P., Arlie, J. P., Convers, A., Mikitenko, P., and Sugier, A., Hydrocarbon Proceedings, Nov. 1984, p. 105.; Chaumette, P., and Hugues, F., *Rev.* I.F.P., **40,** p. 91 (1985); Ohno, T., Yoshimoto, M., Asslineau, L., Courty, P., and Travers, P., 78th Spring National AIChE Meeting, New Orleans, 1986.
5. Hofstadt, C. E., Schneider, M., Bock, O., and Kochloefl, K., *in* Proceedings, III International Symposium: Scientific Bases for the Preparation of Catalysts, Louvain-la-Neuve, Belgium," 1982.
6. Greene, M. J., *Chem. Eng. Progr.* **8,** 46 (1982).
7. Smith, K. J., and Anderson, R. B., *Canad. J. Chem. Eng.* **61,** 40 (1983); Smith, K. J., and Anderson, R. B., *J. Catal.* **85,** 428 (1984).
8. Forzatti, P., Pasquon, I., Villa, P. L., and Vita, G., *Riv. Combust.* **38,** 207 (1984); Pasquon, I.,

Chim. Ind. (Milan) **66,** 700 (1984); Villa, P. L., Forzatti, P., Buzzi-Ferraris, G., Garone, G., and Pasquon, I., *Ind. Eng. Chem. Proc. Des. Dev.* **24,** 12 (1985); Villa, P. L., Del Piero, G., Cipelli, A., Lietti, L., and Pasquon, I., *Appl. Catal.* **26,** 161 (1986); Tronconi, E., Ferlazzo, N., Forzatti, P., and Pasquon, I., *Ind. Eng. Chem. Res.* **26,** 2122 (1987); Tronconi, E., Cristiani, C., Ferlazzo, N., Forzatti, P., Pasquon, I., and Villa, P. L., *Appl. Catal.* **32,** 285 (1987); Villa, P. L., Del Piero, G., Lietti, L., Garagiola, F., Mologni, G., Tronconi, E., and Pasquon, I., *Appl. Catal.*, **35,** 47 (1987).

9. Deluzarche, A., Hindermann, J. P., Kieffer, R., Breault, R., and Kienneman, A., *J. Phys. Chem.* **88,** 4993 (1984); Saussey, J., Lavalley, J. C., Rais, T., Chakoer-Alami, A., Hindermann, J. P., and Kienneman, A., *J. Mol. Catal.* **26,** 159 (1984); Kieffer, R., Kienneman, A., Rodriguez, M., and Hindermann, J. P., IX Iberoamerican Symposium of Catalysis, Lisbon, 1984, p. 1509; Hindermann, J. P., Razzaghi, A., Breault, R., Kieffer, R., and Kienneman, A., *React. Kinet. Catal. Lett.* **26,** 221 (1984); Deluzarche, A., Hindermann, J. P., Kienneman, A., and Kieffer, R., *J. Mol. Catal.* **31,** 225 (1985); Kienneman, A., Hindermann, J. P., Breault, R., and Idriss, H., *Amer. Chem. Soc. Div. Petrol. Chem.* **31,** 46 (1986); Breault, R., Kienneman, A., Hindermann, J. P., and Laurin, M., "Proceedings, 10th Canadian Symposium on Catalysis," June 1986.
10. Maj, J., Colmenares, C. A., and Somorjai, G. A., *J. Catal.* **95,** 385 (1985); Youchang, Xie, Naasz, B. M., and Somorjai, G. A., *Appl. Catal.* **27,** 233 (1986).
11. Fujimoto, K., and Oba, T., *Appl. Catal.* **13,** 289 (1985).
12. Pijolat, M., and Perrichon, V., *Appl. Catal.* **13,** 321 (1985).
13. Takeuchi, K., Matsuzaki, T., Arakaua, H., and Sugi, Y., *Appl. Catal.* **18,** 325 (1985).
14. Holy, N. L., and Carey, T. F., Jr., *Appl. Catal.* **19,** 21 (1985).
15. Thivolle-Cazat, J., *Appl. Catal.* **24,** 211 (1986).
16. Di Conca, M., Riva, A., Trifirò, F., Vaccari, A., Del Piero, G., Fattore, V., and Pincolini, F., *in* "Proceedings, 8th International Congress on Catalysis, Berlin," Vol. 2, p. 173, Dechema, Frankfurt, 1984; Del Piero, G., Trifirò, F., and Vaccari, A., *J. Chem. Soc. Chem. Commun.*, 656 (1984); Riva, A., Trifirò, F., Vaccari, A., Busca, G., Mintchev, L., Sanfilippo, D., and Manzatti, W., *J. Chem. Soc. Faraday Trans. 1,* 2213 (1987); Fornasari, G., Gusi, S., La Torretta, T. M. G., Trifirò, F., and Vaccari, A., *in* "Catalysis and Automotive Pollution Control," p. 469. Elsevier, Amsterdam, 1987.
17. Paggini, A., and Sanfilippo, D., 78th Spring National AIChE Meeting, New Orleans, 1986.
18. Quarderer, G., 78th Spring National AIChE Meeting, New Orleans, 1986.
19. Supp, E., 78th Spring National AIChE Meeting, New Orleans, 1986; Hilsebein, W., 1986 World Methanol Conference, Frankfurt, 1986.
20. Frohlich, P. K., and Lewis, W. K., *Ind. Eng. Chem.* **20,** 354 (1928).
21. Frohlich, P. K., and Cryder, D. S., *Ind. Eng. Chem.* **22,** 1051 (1930).
22. Graves, G. D., *Ind. Eng. Chem.* **23,** 1381 (1932).
23. Morgan, G. T., Hardy, D. V. N., and Procter, R. H., *J. Soc. Chem. Ind. Trans. Commun.* **51,** 1T (1932).
24. Taylor, R. J., *Chem. Soc. (London)*, 1429 (1934).
25. Anderson, R. B., Feldman, J., and Storch, H. H., *Ind. Eng. Chem.* **44,** 2418 (1952).
26. Runge, F., and Zepf, K., *Brennstoff-Chem.* **35,** 167 (1954).
27. Natta, G., Colombo, U., and Pasquon, I., *in* "Catalysis" (P. H. Emmet Ed.), Vol. V, p. 31. Reinhold, New York, 1957.
28. Neczaj-Hruzewicz, J., Janusz, W., and Szczypa, J., *Gazz. Chim. Ital.* **107,** 461 (1977).
29. Hiller, S. A. Karmilchik, A. Ya., Stonkus, V. V., Katayev, B. S., and Shymanska, M. V., *in* "Preparation of Catalysts" (B. Delmon, P. A. Jacobs, and G. Poncelet, Eds.), p. 579. Elsevier, Amsterdam, 1976.
30. Del Piero, G., Di Conca, M., Trifirò, F., and Vaccari, A., *in* "Reactivity of Solids" (P. Barret and L. C. Dufour, Eds.), p. 1029. Elsevier, Amsterdam, 1985.
31. Muller, O., and Ray, R., "The Major Ternary Structural Families." Springer-Verlag, Berlin, 1974.
32. Miller, A., *J. Appl. Phys.* **30,** 24S (1959).